HHS Public Access

Author manuscript

Science. Author manuscript; available in PMC 2016 February 23.

Published in final edited form as:

Science. 2015 August 7; 349(6248): 647–650. doi:10.1126/science.aaa7484.

Natural light-gated anion channels: A family of microbial rhodopsins for advanced optogenetics

Elena G. Govorunova[1], **Oleg A. Sineshchekov**[1], **Roger Janz**[2], **Xiaoqin Liu**[2], and **John L. Spudich**[1,*]

[1]Center for Membrane Biology, Department of Biochemistry and Molecular Biology, University of Texas Medical School, Houston, TX 77030, USA

[2]Department of Neurobiology and Anatomy, University of Texas Medical School, Houston, TX 77030 USA

Abstract

Light-gated rhodopsin cation channels from chlorophyte algae have transformed neuroscience research through their use as membrane-depolarizing optogenetic tools for targeted photoactivation of neuron firing. Photosuppression of neuronal action potentials has been limited by the lack of equally efficient tools for membrane hyperpolarization. We describe anion channel rhodopsins (ACRs), a family of light-gated anion channels from cryptophyte algae that provide highly sensitive and efficient membrane hyperpolarization and neuronal silencing through light-gated chloride conduction. ACRs strictly conducted anions, completely excluding protons and larger cations, and hyperpolarized the membrane of cultured animal cells with much faster kinetics at less than one-thousandth of the light intensity required by the most efficient currently available optogenetic proteins. Natural ACRs provide optogenetic inhibition tools with unprecedented light sensitivity and temporal precision.

Microbial rhodopsins are functionally diverse (1, 2). Several are used as molecular tools for optogenetics to regulate cellular activity with light (3–5). Membrane-depolarizing phototaxis receptors from green (chlorophyte) flagellate algae (6), best known as channelrhodopsins (ChRs) function as millisecond–time scale light-gated cation channels (7, 8) and are widely used to depolarize genetically targeted populations of excitable cells. Hyperpolarizing rhodopsin ion pumps have been used to suppress neuron firing (9–13), but they transport only a single charge per captured photon and therefore have limited capacity. Recently, ChRs were engineered to conduct Cl^-, but these optogenetic tools still retain some cation conductance and could be made highly light-sensitive only at the expense of slowing the channel kinetics with additional mutations (14, 15). Ideal for optogenetic hyperpolarization would be natural light-gated anion channels optimized by evolution to be strictly anion-selective and highly conductive with rapid kinetics.

*Corresponding author. john.l.spudich@uth.tmc.edu.

Supplementary Materials: www.sciencemag.org/content/349/6248/647/suppl/DC1

Of the ∼50 known ChRs from chlorophytes, all that have been tested are exclusively cation channels (7, 8, 16–18). Photoreceptor currents similar to those mediated by ChRs in chlorophytes also occur in the phylogenetically distant cryptophyte algae (19). However, several rhodopsin proteins from genes cloned from these organisms did not exhibit channel activity (19, 20). The nuclear genome of the cryptophyte *Guillardia theta* has been completely sequenced (21). A BLAST search of model proteins identified 53 with sequence similarity to that of microbial (type I) rhodopsins. None showed high similarity to ChRs, but the models of one particular cluster (Fig. 1A and fig. S1) did contain some key residues characteristic of chlorophyte ChRs (Fig. 1B and fig. S2).

Gene fragments encoding seven transmembrane domains of *G. theta* proteins 111593,146828, and 161302 were well expressed in transfected human kidney embryonic (HEK293) cells. The first two constructs generated photocurrents, whereas the third did not. The first two functioned as light-gated anion channels; therefore we named them *Gt*ACR1 and *Gt*ACR2 (*Guillardia theta* anion channel rhodopsins 1 and 2).

With our standard solutions for electrophysiological recording (126 mM KCl in the pipette and 150 mM NaCl in the bath, pH 7.4; for other components see table S1), the currents generated by *Gt*ACR1 and *Gt*ACR2 were inward at the holding potential (E_h) of −60 mV (Fig. 1D). The mean plateau currents from *Gt*ACR1 and *Gt*ACR2 were, respectively, eight and six times larger than those from *Cr*ChR2 (*Cr*, *Chlamydomonas reinhardtii*), the most frequently used optogenetic tool, with a lesser degree of inactivation (Fig. 1, inset). The dependence of the current rise rate on the stimulus intensity exhibited a higher saturation level than the current amplitude (Fig. 1E) and therefore was used for construction of the action spectra. *Gt*ACR1 showed maximal sensitivity to 515-nm light, with a shoulder on the short-wavelength slope of the spectrum (Fig. 1F). The sensitivity of *Gt*ACR2 peaked at 470 nm, with additional bands at 445 and 415 nm (Fig. 1F).

The sign of *Gt*ACR1 and *Gt*ACR2 photocurrents reversed when the membrane potential was shifted to more positive values (Fig. 2, A and B, respectively). In the tested range from −60 to 60 mV, the current-voltage relationships (*IE* curves) were linear (Fig. 2C), unlike those for chlorophyte ChRs (22). To characterize the ion permeability of *G. theta* rhodopsins, we measured *IE* curves and determined the reversal potential (E_{rev}) upon variation of the ionic composition of the bath solution. In contrast to chlorophyte ChRs, for which protons are the most highly permeable ions, E_{rev} of the currents generated by *Gt*ACR1 and *Gt*ACR2 were not affected by pH (Fig. 2C). Moreover, no E_{rev} shifts were observed when the large nonpermeable organic cation *N*-methyl-glucamine (NMG^+) was replaced with Na^+, K^+, or Ca^{2+} (Fig. 2D). We conclude that *Gt*ACR1 and *Gt*ACR2 are not permeable by cations conducted by chlorophyte ChRs.

When most of the Cl^- in the bath was replaced with the large anion aspartate, yielding a Nernst equilibrium potential for Cl^- (E_{Cl}) of 81 mV, E_{rev} shifted to 75 ± 2.4 and 80 ± 1.4 mV (mean ± SEM, n = 4 to 5 cells) for *Gt*ACR1 and *Gt*ACR2, respectively (Fig. 3C), as would be expected only if the currents were exclusively due to passive Cl^- transport. We compared the permeability of various anions by substituting them for nonpermeable Asp^- in the bath. For both *G. theta* ACRs, I^-, NO_3^-, or Br^- caused even greater E_{rev} shifts than Cl^-.

F^- caused a smaller shift, whereas SO_4^{2-} was nonpermeable. The permeability sequence $NO_3^- > I^- > Br^- > Cl^- > F^- > SO_4^{2-} = Asp^-$ determined for ACRs is in accord with the lyotropic series characteristic of many Cl^- channels from animal cells (23).

The cytoplasmic Cl^- concentration in most animal cells, including neurons, is low (24). Under such conditions (5 mM Cl^- in the pipette and 156 mM in the bath), *G. theta* ACRs generated hyperpolarizing currents in HEK293 cells at E_h above the Nernst equilibrium potential for Cl^- (E_{Cl}) (fig. S3). The amplitude of *Gt*ACR2 photo-currents was similar, but the kinetics was faster than that of *Gt*ACR1 currents, which is advantageous for control of neuronal activity. Hyper-polarizing photocurrents generated by *Gt*ACR2 at the less-than-1000th lower light intensity were equal to the maximal currents generated by the proton pump archaerhodopsin-3 (Arch), a popular tool for optogenetic spike suppression (12), and by the recently reported slow ChloC mutant (14) (Fig. 4A, black arrow). The stimulus-response curve for the mutant was less steep than for *Gt*ACR2 because of the slower current kinetics of the latter (Fig. 4E). However, even at nonsaturating light intensities, *Gt*ACR2 remained more than 100 times more photosensitive than slow ChloC (Fig. 4A, red arrow). The larger amplitude of *Gt*ACR2 photocurrents was not due to its higher expression level, as assessed by measuring relative tag fluorescence (fig. S4). Higher unitary conductance of ACRs is shown by stationary noise analysis of macroscopic current fluctuations, which gave values for *Gt*ACR1 and *Gt*ACR2 more than 10 times higher than those for *Cr*ChR2 (fig. S5) (25).

In cultured rat pyramidal neurons, *Gt*ACR2 generated hyperpolarizing currents at E_h above -88 mV (Fig. 4B and fig. S6A). This value corresponds exactly to E_{Cl} under our conditions (table S2). This strict selectivity is a second advantage of ACRs over the previously reported Cl^--conducting ChR mutants, for which E_{rev} is 25 to 30 mV more positive than E_{Cl}, due to residual cation permeability (14, 15). The range of potentials at which *Gt*ACR2 hyperpolarizes the membrane is therefore wider and extends through the values typical for resting potentials of neurons (Fig. 4B). In current clamp experiments, *Gt*ACR2 allowed precisely controlled optical silencing of spikes at frequencies up to at least 25 Hz (Fig. 4C and fig. S6B).

To compare the efficiency of *Gt*ACR2 with that of slow ChloC in neurons, we measured the rheobase of current ramp-evoked spikes at different light intensities using the same solutions and current injection protocol as in (14). In *Gt*ACR2-expressing neurons, full suppression of spiking was observed at 0.005 mW/mm^2 (Fig. 4D). The fast ChloC mutant, comparable in its kinetics to *Gt*ACR2, could not fully suppress spiking even at 10 mW/mm^2 of light, whereas a relatively higher efficiency of slow ChloC with full suppression at ~0.1 mW/mm^2 (the reciprocal of this value is plotted in the Fig. 4D, inset) was achieved only at the expense of a dramatically slower kinetics and the necessity to illuminate for at least 12 s (14) (Fig. 4E). As *Gt*ACR2-driven current reached its maximum within 0.1 s (Fig. 4E), its intensity dependence at any length of the light pulse above 0.1 s was identical to that shown in Fig. 4A In contrast, the rise of current generated by slow ChloC was 65 times slower (Fig. 4E). Taking into account the intensity dependence of the current amplitude measured with light stimuli of different duration (Fig. 4F), full suppression of spiking by slow ChloC with

0.1-s stimuli would occur at 7 mW/mm^2, whereas by *Gt*ACR2 it would be reached at an intensity about three orders of magnitude lower.

The membrane potential, membrane resistance, and rheobase in the dark were not affected by *Gt*ACR2 expression in neurons, and the neuronal morphology of *Gt*ACR2-expressing neurons was also normal (fig. S7).

Phylogenetically and functionally, ACRs constitute a distinct family of rhodopsins that are fundamentally different from cation channel-rhodopsins (CCRs). As natural anion channels, ACRs provide hyperpolarizing optogenetic tools optimized by evolution for extremely high light sensitivity, absolute anion selectivity, and rapid kinetics.

Supplementary Material

Refer to Web version on PubMed Central for supplementary material.

Acknowledgments

E.G.G., O.A.S., J.L.S., and The University of Texas Health Science Center at Houston have filed a provisional patent application that relates to ACRs. We thank E. S. Boyden [Massachusetts Institute of Technology (MIT), Boston] for the archaeorhodopsin-3 expression construct and C. Lois (MIT) for the pCMV-VSVG and pΔ8.9 plasmids. This work was supported by NIH grants R01GM027750, R21MH098288, and S10RR022531, and a UTHealth BRAIN Initiative grant, the Hermann Eye Fund, and Endowed Chair AU-0009 from the Robert A. Welch Foundation.

References and Notes

1. Spudich JL, Sineshchekov OA, Govorunova EG. Biochim Biophys Acta. 2014; 1837:546–552. [PubMed: 23831552]
2. Ernst OP, et al. Chem Rev. 2014; 114:126–163. [PubMed: 24364740]
3. Deisseroth K. Nat Methods. 2011; 8:26–29. [PubMed: 21191368]
4. Chow BY, Boyden ES. Sci Transl Med. 2013; 5:177ps5.
5. Lin JY, Knutsen PM, Muller A, Kleinfeld D, Tsien RY. Nat Neurosci. 2013; 16:1499–1508. [PubMed: 23995068]
6. Sineshchekov OA, Jung KH, Spudich JL. Proc Natl Acad Sci USA. 2002; 99:8689–8694. [PubMed: 12060707]
7. Nagel G, et al. Science. 2002; 296:2395–2398. [PubMed: 12089443]
8. Nagel G, et al. Proc Natl Acad Sci USA. 2003; 100:13940–13945. [PubMed: 14615590]
9. Zhang F, et al. Nature. 2007; 446:633–639. [PubMed: 17410168]
10. Han X, Boyden ES. PLOS ONE. 2007; 2:e299. [PubMed: 17375185]
11. Gradinaru V, Thompson KR, Deisseroth K. Brain Cell Biol. 2008; 36:129–139. [PubMed: 18677566]
12. Chow BY, et al. Nature. 2010; 463:98–102. [PubMed: 20054397]
13. Chuong AS, et al. Nat Neurosci. 2014; 17:1123–1129. [PubMed: 24997763]
14. Wietek J, et al. Science. 2014; 344:409–412. [PubMed: 24674867]
15. Berndt A, Lee SY, Ramakrishnan C, Deisseroth K. Science. 2014; 344:420–424. [PubMed: 24763591]
16. Zhang F, et al. Cell. 2011; 147:1446–1457. [PubMed: 22196724]
17. Govorunova EG, Sineshchekov OA, Li H, Janz R, Spudich JL. J Biol Chem. 2013; 288:29911–29922. [PubMed: 23995841]
18. Klapoetke NC, et al. Nat Methods. 2014; 11:338–346. [PubMed: 24509633]

19. Sineshchekov OA, et al. Biophys J. 2005; 89:4310–4319. [PubMed: 16150961]
20. Gradinaru V, et al. Cell. 2010; 141:154–165. [PubMed: 20303157]
21. Curtis BA, et al. Nature. 2012; 492:59–65. [PubMed: 23201678]
22. Gradmann D, Berndt A, Schneider F, Hegemann P. Biophys J. 2011; 101:1057–1068. [PubMed: 21889442]
23. Jentsch TJ, Stein V, Weinreich F, Zdebik AA. Physiol Rev. 2002; 82:503–568. [PubMed: 11917096]
24. Bregestovski P, Waseem T, Mukhtarov M. Front Mol Neurosci. 2009; 2:15. [PubMed: 20057911]
25. Feldbauer K, et al. Proc Natl Acad Sci USA. 2009; 106:12317–12322. [PubMed: 19590013]

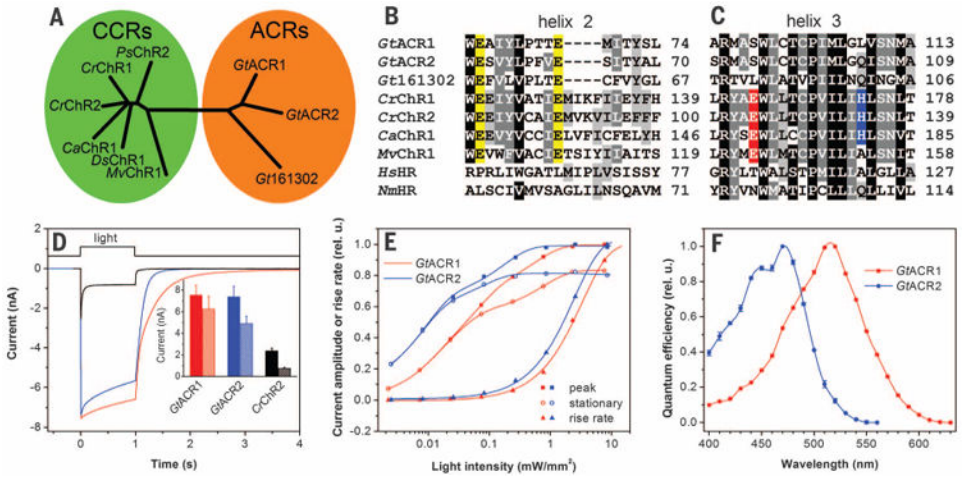

Fig. 1. Phylogeny and photoactivity of *G. theta* ACRs

(**A**) Phylogenetic tree of CCRs and ACRs. (**B** and **C**) ClustalW alignments of transmembrane helices 2 (**B**) and 3 (**C**) Abbreviated organism names are: *Gt Guillardia theta; Cr Chlamydomonas reinhardti*i; *Ca Chlamydomonas augustae; Mv Mesostigma viride; Hs, Halobacterium salinarum; Nm, Nonlabens marinus.* The last residue numbers are shown on the right. Conserved Glu residues in helix 2 are highlighted in yellow, Glu residues in the position of bacteriorhodopsin Asp85 in red, and His residues corresponding to His134 of *Cr*ChR2 in blue. (**D**) Photocurrents of *Gt*ACR1, *Gt*ACR2, and *Cr*ChR2 in HEK293 cells in response to a saturating light pulse at −60 mV. (Inset) Mean amplitudes of peak (solid bars) and stationary (hatched bars) currents (n = 18 to 20 cells). (**E**) Dependence of the peak and stationary current amplitudes and rise rates on stimulus intensity. (**F**) Action spectra of photocurrents.

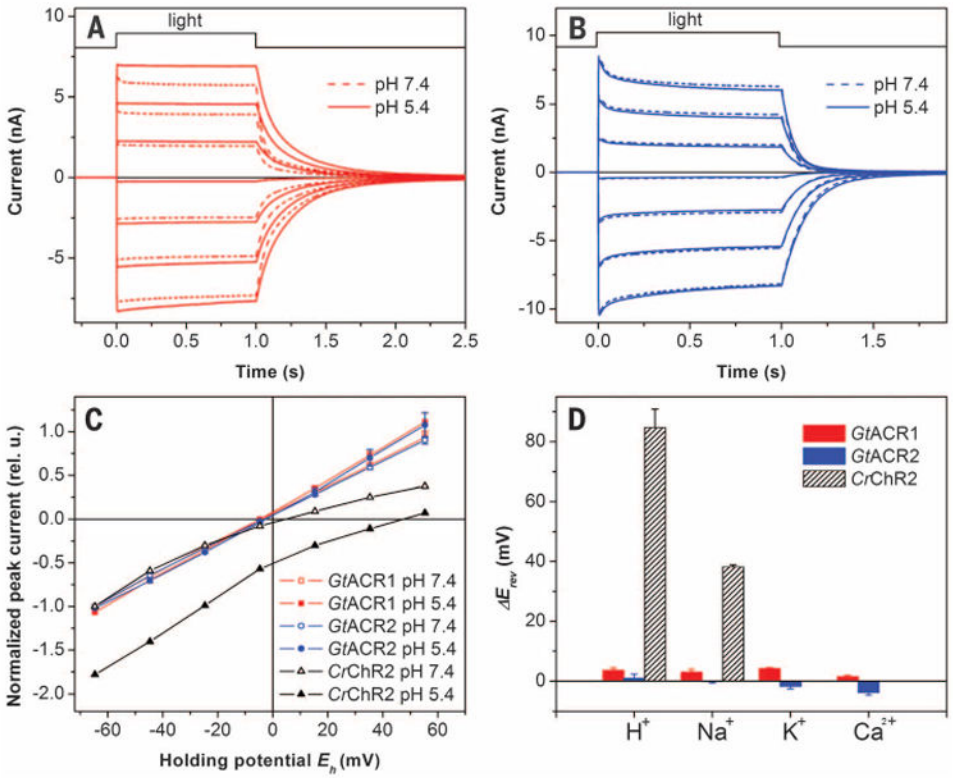

Fig. 2. ACRs do not conduct cations

Photocurrents generated by *Gt*ACR1 (**A**) and *Gt*ACR2 (**B**) in HEK293 cells at the membrane potentials changed in 20-mV steps from −60 mV at the amplifier output (bottom to top). The pipette solution was standard, and the bath solution was as indicated. (**C**) *IE* relationships measured at various pH of the bath. The data (mean values ± SEM, n = 4 to 6 cells) were corrected for liquid junction potentials (table S1) and normalized to the value measured at −60 mV at pH 7.4. Representative data for *Cr*ChR2 are shown for comparison. (**D**) E_{rev} shifts measured upon variation of the cation composition of the bath. The data are mean values ± SEM (n = 3 to 6 cells).

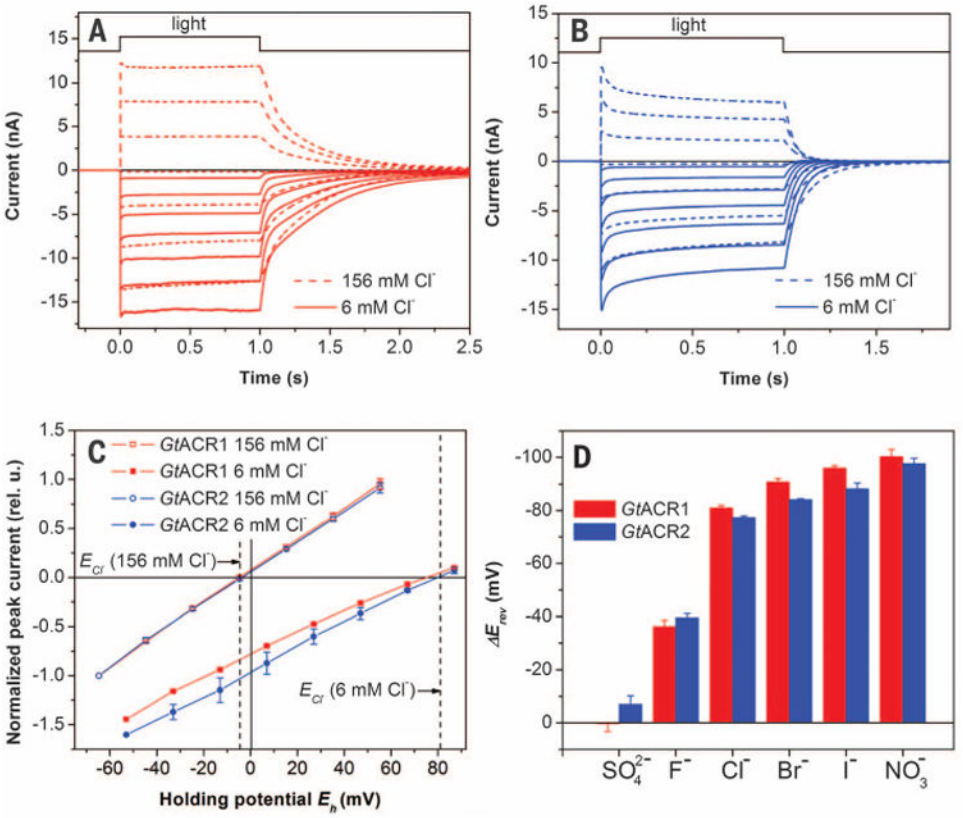

Fig. 3. Anion selectivity of ACRs

Photocurrents generated by *Gt*ACR1 (**A**) and *Gt*ACR2 (**B**) in HEK293 cells at the membrane potentials changed in 20-mV steps from −60 mVat the amplifier output (bottom to top). The pipette solution was standard, and the bath solution was as indicated. (**C**) *IE* relationships measured at various Cl^- concentrations in the bath. The data (mean values ± SEM, n = 4 to 6 cells) were corrected for liquid junction potentials (table S1) and normalized to the value measured at −60 mV at 156 mM CI^-. The dashed vertical lines show the Nernst equilibrium potential for Cl^- at the bath concentrations used. (**D**) E_{rev} shifts measured upon variation of the anion composition of the bath. The data are mean values ± SEM (n = 3 to 6 cells).

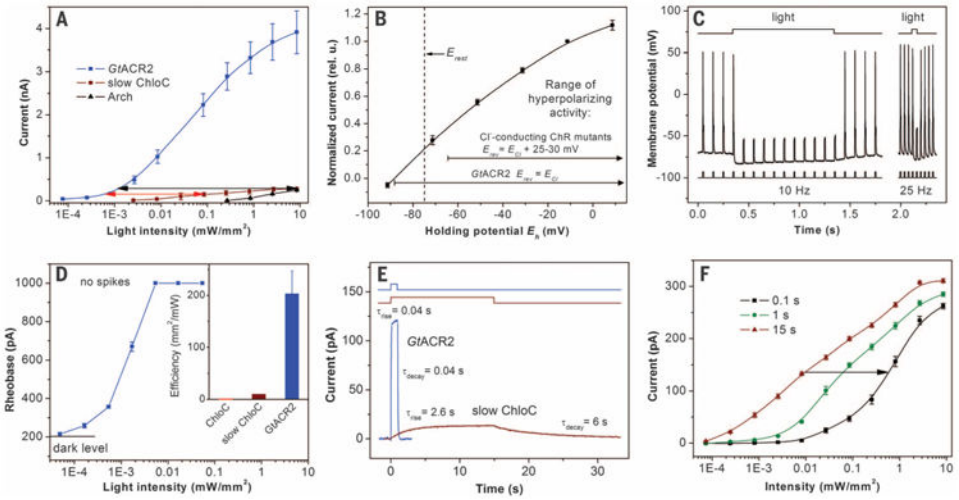

Fig. 4. *Gt*ACR2 as a hyperpolarizing tool

(**A**) Light-intensity dependence of photocurrents generated by *Gt*ACR2, slow ChloC, and Arch in HEK293 cells at 20 mV. The arrows show the difference in light sensitivity. (**B**) *IE* relationship for *Gt*ACR2 in neurons. The data (mean values ± SEM, n = 5 cells) were corrected for LJP (table S2). The dashed vertical line shows the resting potential (E_{rest}). The ranges of activity for Cl^--conducting ChR mutants are from (14, 15). (**C**) Photoinhibition of spiking induced by pulsed current injection in a typical neuron expressing *Gt*ACR2. The light intensity was 0.026 mW/mm^2. (**D**) The dependence of the rheobase of current ramp-evoked spikes on the light intensity in a typical neuron expressing *Gt*ACR2. The data are mean values ± SEM (n = 5 repetitions). Light was applied 0.1 s before the beginning of the current ramp. (Inset) Comparative efficiency of *Gt*ACR2 and the ChloC mutants represented as a reciprocal of the minimal light intensity sufficient to fully suppress spiking. The data for *Gt*ACR2 are the mean value ± SEM (n = 7 neurons). Data for the ChloC mutants under continuous illumination are from (14). (**E**) Kinetics of the photocurrents generated by *Gt*ACR2 in response to a 1-s light pulse and by slow ChloC in response to a 15-s light pulse (light intensity for both traces was 0.002 mW/mm^2). The time constants (τ) were determined by single exponential fits of the recorded traces. The fitted curves are shown as thick lines of the same color as the data. (**F**) The light-intensity dependence of slow ChloC current amplitude measured at different times after the start of illumination. Data are mean values ± SEM (n = 5 cells). The arrow shows the increase in the light intensity necessary to reach the same current amplitude at 0.1 as at 15 s illumination.